The 8th International Supercritical CO_2 Power Cycles Symposium
February 27 – 29, 2024, San Antonio, Texas
Paper #28

Effects of Near-critical Inlet Condition on the Performance of Supercritical CO_2 Compressor

Wenlin Xie
Master Student
School of Aeronautics and Astronautics,
University of Chinese Academy of Science
Key Laboratory of Advanced Energy and Power,
Institute of Engineering Thermophysics, Chinese Academy of Sciences
Beijing, China

Yong Tian
Associate Research Fellow
School of Aeronautics and Astronautics,
University of Chinese Academy of Science
Key Laboratory of Advanced Energy and Power,
Institute of Engineering Thermophysics, Chinese Academy of Sciences
Beijing, China

Bo Wang
Associate Research Fellow
School of Engineering Science, University of Chinese Academy of Science
Key Laboratory of Advanced Energy and Power,
Institute of Engineering Thermophysics, Chinese Academy of Sciences
Beijing, China

Xiang Xu
Director
School of Engineering Sciences, University of Chinese Academy of Science
Key Laboratory of Advanced Energy and Power,
Institute of Engineering Thermophysics, Chinese Academy of Sciences
Beijing, China

ABSTRACT

The supercritical carbon dioxide (sCO_2) Brayton cycle efficiency increase as the compressor inlet condition approaches the critical point of CO_2. However, the thermodynamic properties of CO_2 change dramatically near the critical point, what is more, phase-change is most likely to happen. Both cavitation and condensation bring about significant adverse effects to the performance of compressor. In this paper, considering the models of cavitation and condensation, the quantitative effect of nonequilibrium phase-change on the performance of sCO_2 centrifugal compressor with different inlet relative entropy will be investigated. In Ansys Fluent numerical investigation, the properties of CO_2 are provided by real gas properties table and nonequilibrium phase-change model is adopted. The approach of modeling two-phase flow with nonequilibrium phase-change model is validated by using test data in a De Laval nozzle and Sandia compressor. It is shown that condensation onset, Wilson line, and the performance curve are well predicted. Finally, a simulation is carried out in the two-stage centrifugal compressor for an 8MWt sCO_2 power cycle test rig. When inlet relative entropy is lower than one, fluid behaves like liquid. The compressor has a large pressure ratio and small temperature rise, reflecting the characteristics of pump. In the first stage, cavitation and condensation will occur simultaneously at leading edge of the blade. But cavitation dominates. As the relative entropy approaches one, the cavitation is more severe, the pressure ration decreases and temperature rise increase. When relative entropy is greater than one, working fluid behaves like gas and condensation dominates. If the relative entropy is still increasing, the stable operating range of the compressor will narrow rapidly.

INTRODUCTION

With the growing problem of energy scarcity and the increase of people's awareness of

environmental protection, the society places a great emphasis on the efficient and environmentally friendly power cycle. Various countries are now developing clean and renewable energy, reducing greenhouse gas and harmful gas emissions, optimizing current energy systems and improving cycle efficiency.

The Brayton cycle of supercritical carbon dioxide (sCO_2) is an attractive power generation technology, which offers potential advantage in terms of cycle efficiency. As for working fluid, CO_2 has good stability, abundant storage. In supercritical state, CO_2 has high specific heat capacity, large isothermal compressibility, high density, low viscosity and other qualities. These features can significantly reduce the compression work and then improve the cycle efficiency. The closer the inlet condition approaches the critical point, the greater the system performance is[1]. However, when the compressor inlet condition approaches the critical point, the thermophysical properties of CO_2 will change dramatically, deviate significantly from the ideal gas and show a strong real gas effect[2]. On the other hand, critical point is the end of saturation line. When the compressor inlet condition is near the critical point, the phase change may be triggered in the impeller blade channel due to the local flow acceleration. The phase change usually occurred on the suction side. The droplets in impeller blade may further deteriorate the performance of compressor or cause the erosion. Also, it is possible that the temperature and pressure of sCO_2 fluid decrease below the critical point and pass through the saturation line, causing the phase change under the compressor's start-stop and off-design settings. At present, there are very few experiments on the flow and phase-change. The studies of Sandia National Laboratories have shown that the compressor can work stably no matter which phase the inlet condition of the sCO_2 compressor is[3]. Noall[4] believed that the compressor can achieve a long-term table operation with a two-phase inlet condition, which is limited to the low rotational speed. The preceding investigations are concerned with the overall performance of the compressor and do not provide a clear picture of the specific internal-flow characteristic of sCO2 the compressor. It is still difficult to measure the internal flow through experiments, due to the small size of impeller. Although some studies state that phase-change has little effect on the compressor performance, most studies consider potential two-phase operation as a high risk and do not recommend for a high reliability system[5]. Therefore, it is necessary to investigate the quantitative effect of near-critical nonequilibrium phase-change on the performance of sCO_2 centrifugal compressor, so as to improve theoretical guidance for the design and operation strategy of sCO_2 compressor.

NUMERICAL INVESTIGATION

The internal flow of sCO_2 centrifugal compressor in approximately isentropic flow with local expansion process. Therefore, numerical simulations under various different near-critical conditions can be carried out in a relatively simple geometric model, which is the Laval nozzle. The simulations are to test the reliability of the non-equilibrium phase-change model and corresponding two-phase flow simulation method. The characteristics of non-equilibrium phase-change flow filed are analyzed and the results are compared with the experimental data of Lettieri[6]. The experimental test apparatus consists of a blowdown test rig, which is filled with high pressure CO_2. The exhaust gas flows through the Laval nozzle. The nozzle length is 91.3mm, the throat area is 20mm^2, the height of throat is 3.09mm, and the distance from the throat to the exit is 61.3mm. The inlet to throat and outlet to throat area ratios are 4.1 and 1.3 respectively. Fig 1 shows the grid of the nozzle. The real gas properties table bounds vary from (220k, 0.1MPa) to (400k, 30MPa). There are 500 temperature, pressure and saturation points in the table.

In the numerical procedure, Fluent was used as the numerical solver of mesh model to solve the

governing equations and addition nonequilibrium phase-change model. Two turbulence equation of k−ω SST model was applied to calculate the turbulence characteristics of flow. The coupled algorithm was utilized for the coupling of pressure-velocity field and the second-order upwind discretization was used for continuity, momentum and energy equation. Boundary conditions were set as adiabatic, no-slip, smooth wall. Inlet and outlet boundary conditions were set as pressure boundary conditions. When the relative residuals of energy and other dependent variables were less than 10^{-6} respectively and the mass flow rate between the inlet and outlet was less than $1e^{-4}$, the numerical program could be considered to converge. The inlet conditions are shown in table 1, which is the same with the Lettieri experiment[7]. The inlet vapor volume fraction was set as 1.

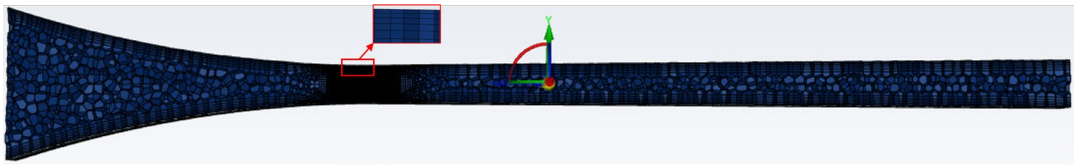

Fig.1 Grid of Laval Nozzle

Table 2 Inlet condition of nozzle

Case	P_t （MPa）	T_t （K）	S （$J/kg \cdot K$）	P_t/P_C	T_t/T_C	S_t/S_C
1	5.9	310	1830	0.8	1.02	1.28
2	6.7	310	1766	0.9	1.02	1.23
3	7.4	310	1695	1.0	1.02	1.18
4	8.0	311	1634	1.1	1.025	1.13
5	8.4	312	1548	1.2	1.027	1.08

Nozzle with different Lee model coefficients were simulated under the inlet condition with relative entropy of 1.18, and pressure profile in nozzle for various Lee Model coefficient values is illustrated in Fig 2. The throat is located at x/L=0, the Y-axis is the normalized pressure using the inlet total pressure. When the Lee model coefficient is 10 or 0.1, the effect on the flow field is almost insignificant and the pressure profile is the same with the profile without phase-change. If the coefficient is 10^6, the effect on the flow field is too strong. The pressure deviates from the experimental data and the flow will approach equilibrium soon, which beaves like equilibrium condensation. Finally, the coefficient of $1e^4$ is adopted in this paper. The pressure profile with this coefficient matches the experiment data very well, which manifests as nonequilibrium condensation.

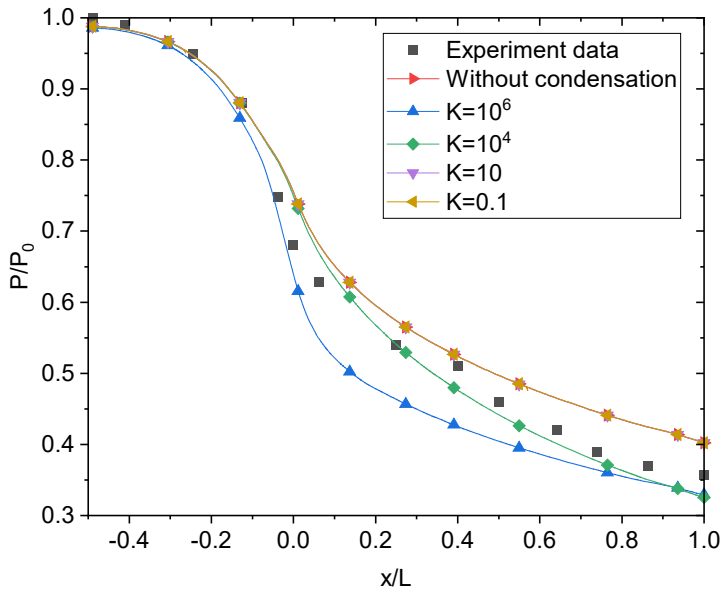

Fig 2 Pressure profile in nozzle for various Lee Model coefficient values

As the high-pressure CO_2 fluid expands and accelerates in the throat, the fluid speeds up into supersonic flow with a decrease in temperature and pressure. When the fluid enters the liquid region, the condensation occurs. Fig 3 compares the condensation onset between the experiment result and numerical simulations. Fig (a) shows the results of Lettieri experiment. The white region is the condensation place of CO_2, the black region is the non-condensation region and the red line indicates the throat. Fig (b) is the contour of the liquid CO_2 volume fraction predicted by Brinckman[8]. When the relaxation time coefficient in the Lee model approaches infinity, the fluid phase transition rate approaches infinity as well. Condensation will occur as long as the fluid passes through the saturation line, which can be regarded as an equilibrium phase-change model. Fig (c) is the contour of the liquid CO_2 volume fraction with a smaller relaxation time coefficient, which is the result of nonequilibrium condensation simulation. Fig (d) is the contour of the liquid CO_2 volume fraction with a bigger relaxation time coefficient, which is the result of equilibrium condensation simulation. The numerical simulation can better predict the trend of condensation onset with various inlet pressures. Also, the prediction results in this paper are more accurate than Brinckman, which due to the high precision real gas property table and nonequilibrium condensation model. The RGP table contains the subcritical and supercritical thermophysical properties and fully considers the thermophysical properties of the two-phases region. The supercritical thermophysical properties can be read directly from the table and have sufficient resolution near the critical point. For the properties of metastable region, the thermophysical properties will be interpolated. Secondly, the simulation considers the nonequilibrium condensation model. When the fluid pass through the saturation line, the condensation will not occur immediately but after a certain relaxation time. As the picture indicates, the condensation onset will move to the throat with the increasing of inlet pressure. The throat has a small area and the density will change drastically. The difficulty of convergences will also increase and the prediction of case 5 deviates from the experiment data a bit more. Comparing the fig (c) to (d), the condensation onset of equilibrium condensation model is closer to throat and has a larger amount of liquid CO_2 volume fraction.

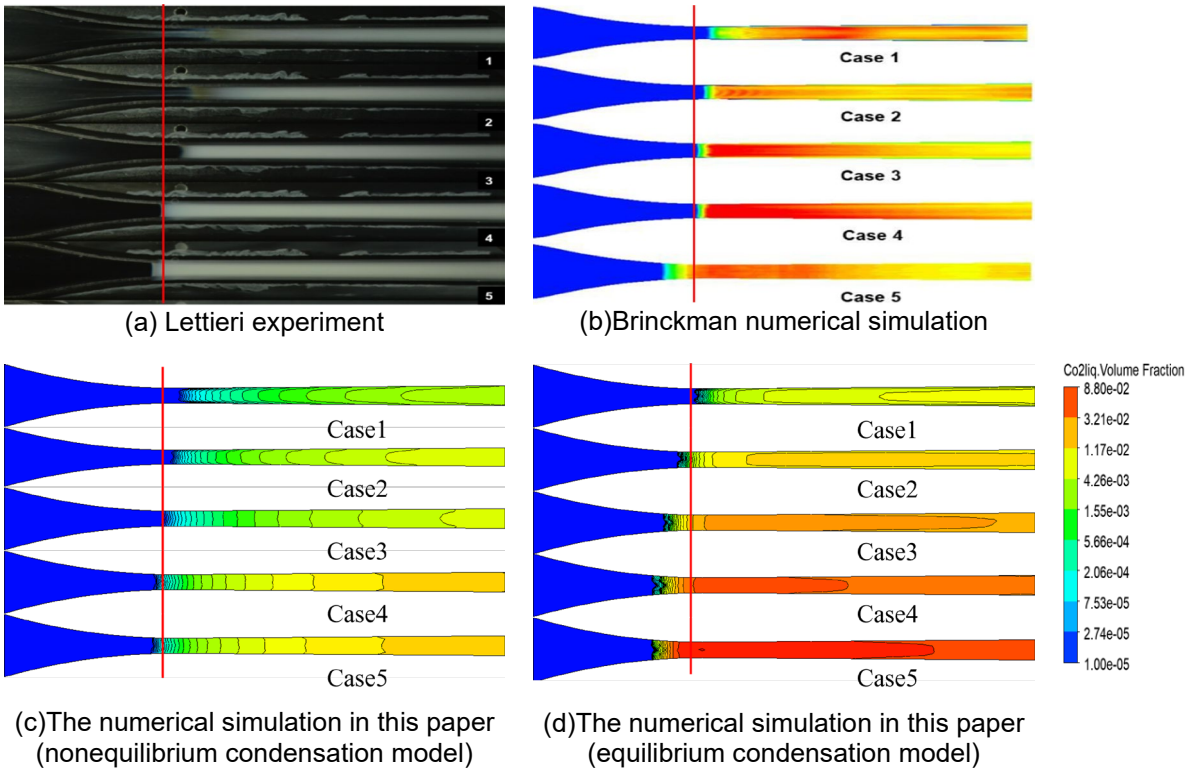

(a) Lettieri experiment (b)Brinckman numerical simulation

(c)The numerical simulation in this paper (nonequilibrium condensation model) (d)The numerical simulation in this paper (equilibrium condensation model)

Fig.3 Comparison of condensation onset

Fig 4 is the comparation of temperature and pressure contours between nonequilibrium condensation model and equilibrium condensation model in case 3. The temperature and pressure are 294.97k and 5.96MPa respectively which are measured at the condensation onset of equilibrium condensation model. The saturation pressure of 294.97k is 5.97MPa, which is slightly higher. Considering how the RGP table works, the temperature and pressure are estimated by interpolation and will be some errors. Therefore, this point can be regarded locating at the saturation line. However, the temperature and pressure are 286.47k and 5.31MPa respectively in nonequilibrium condensation model. The pressure is much lower than the saturation pressure of 286.74k, which means this point is far from the saturation line. As a result, the CO_2 fluid will not condense immediately after passing through the saturation line but instead continues to expand isentropically as a gas form below the critical point before condensation occurs.

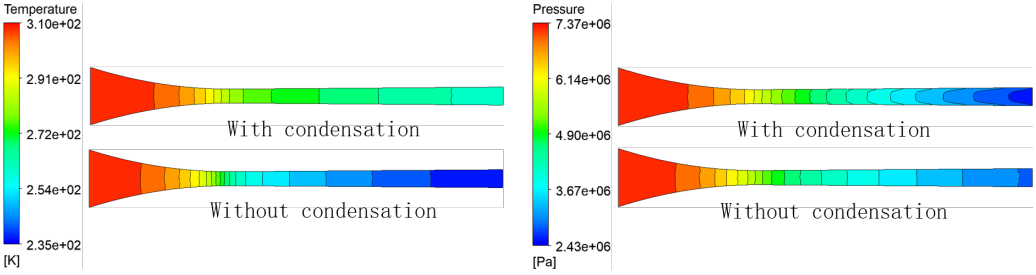

Fig.4 Contour maps of temperature and pressure

Fig 5 depicts a quantitative comparison of condensation onset. The numerical calculation prediction findings are closer to the throat than the experimental data, and the curve distribution

variations follow a similar pattern. The nozzle flow field is unstable in the modeling of non-equilibrium phase change condensation, but the condensation onset is dictated by thermodynamic conditions, thus it can be considered practically unchanged.

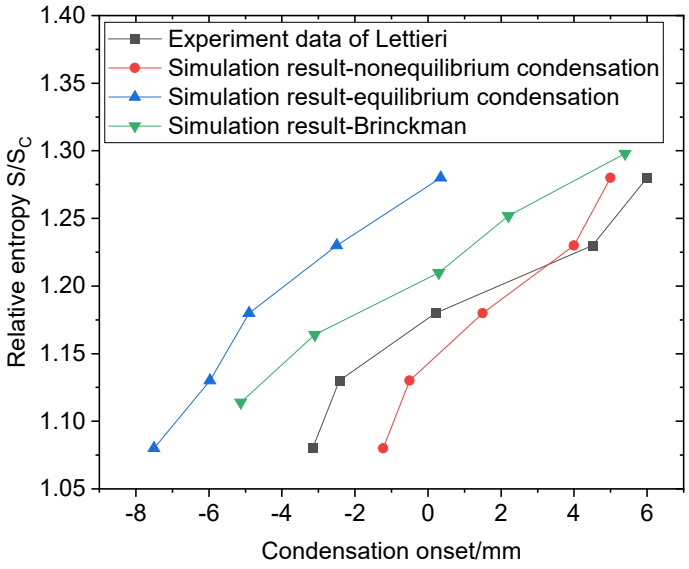

Fig.5 Quantitative comparison of condensation onset

The Wilson line is plotted using the data in Fig 5. Fig 6 shows the Wilson line computed from Fluent compared with test data from experiment. These two lines have a similar trend and the simulation prediction is closer to the throat. As the inlet entropy approaches the critical point, the difference between them decreases because condensation occurs faster at this point. The non-equilibrium condensation phenomena is more drastic with increasing inlet entropy, and the condensation shows noticeable hysteresis. The degree of subcooling before condensation is underestimated by the Fluent numerical simulation. In comparison to the Lettieri experimental results, the non-equilibrium phase-change model and associated two-phase flow simulation method employed above are reliable and can be used for the compressor research that follows.

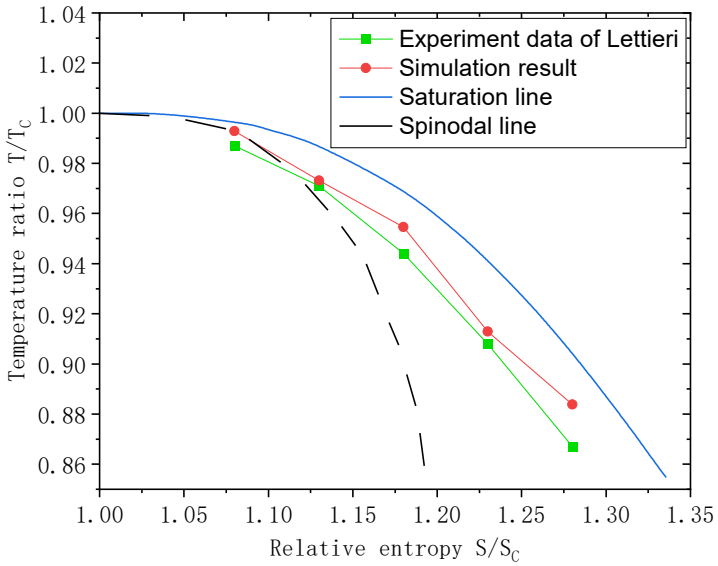

Fig.6 Wilson line computed from Fluent compared with test data from experiment

SANDIA COMPRESSOR

Sandia laboratory previously conducted the sCO_2 centrifugal compressor experiment and published more comprehensive geometric parameters and experimental data[3]. This section mainly focuses on this compressor and carries out numerical simulation. The the one-dimensional and three-dimensional model of the compressor has been reconstructed, according to geometry parameters released by Sandia laboratory. The design inlet total pressure is 7.678MPa, total temperature is 305.3k, mass flow rate is 3.53kg/s, rotation speed is 75krpm, pressure ratio is 1.818 and efficiency is 66.38%. Because the operating temperature and pressure range of the Sandia compressor are identical to those of the Lettieri nozzle experiment, the same real gas property table can be employed. The geometry parameters of the compressor impeller are shown in Table 3. Figure 7 depicts a comparison of the prototype and reconstructed Sandia compressor impeller.

Table 3 Geometry parameters of Sandia main compressor impeller

Parameters	Value	Parameters	Value
Number of main blades	6	Number of splitters	6
Inlet hub radius (mm)	2.537	Inlet shroud radius (mm)	9.372
Inlet hub angle at tip (°)	17.88	Inlet blade angle at tip (°)	50
Exit blade radius (mm)	18.682	Exit blade width (mm)	1.954
Tip clearance (mm)	0.254	Blade thickness (mm)	0.762
Exit blade back sweep angle (°)	-50	Shaft length (mm)	15.9

Fig.7 Geometry of Sandia impeller: (left) original prototype; (right) reconstructed impeller mesh

Due to the difficulty of modeling the sCO_2 centrifugal compressor, the drastic change of thermophysical properties and various inlet conditions, it is challenging to simulate and compare all of the experiment data. Additionally, the experimental data at the speed of 50krm is more comprehensive in the publicly data. Therefore, the simulation shaft speed is set to 50krpm. The same numerical solver was adopted. Two turbulence equation of k−ω SST model was applied, the coupled algorithm was utilized for the coupling of pressure-velocity field. The inlet boundary condition was set as 305.3K and 7.687MPa. The outlet was set as mass flow outlet. Since strong temperature gradients are not present in the flow field and the assumption of adiabatic walls was used. No slip boundary conditions were taken into account on the walls, and constant rotate speed was applied on the hub and impeller.

The comparison between experiment data and result by CFD simulation are shown in Fig. 8, the trends of pressure ratio and efficiency of numerical simulation are close to the experiment data. With the increase of mass flow rate, the pressure ratio of the compressor decreases gradually, and the efficiency increases first before decreasing. The maximum error could result from choosing the vanless diffuser during the simulation procedure rather than the numerical vaned diffuser. Furthermore, the volute is not taken into account during the simulation and only some

parameters of the compressor are given in the Sandia report. There may be some differences between the simulated impeller geometry and the prototype of impeller. The above reasons lead to a little deviation from the experimental results.

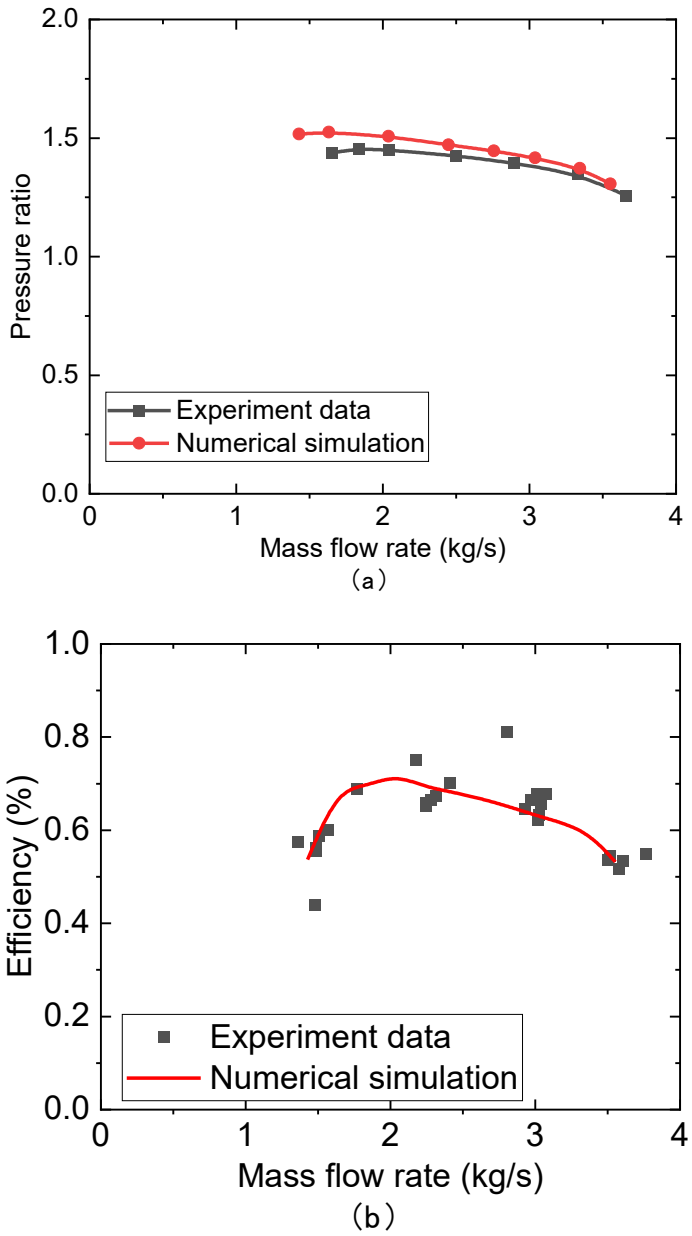

Fig.8 Comparison of performance curve calculated to experiment:(a) pressure ration;(b) efficiency

The contour of 0.5 span's pressure, temperature and liquid CO_2 volume fraction are presented in Fig. 9. The mass flow rate was 2.543kg/s. As shown in Fig.9 average total pressure and temperature increase gradually along the blade passage without obvious saltation, which indicates the relatively homogeneous flow field and well-organized blade profile. The pressure ranges from 6.792MPa to 10MPa and the temperature ranges from 295.8K to 313.5K. Both of the minimum temperature and pressure are lower than the critical point. The low-pressure and low-temperature regions are found at the leading-edge suction sides of blades. The regions result from the flow acceleration around the suction side of the blade leading edge due to the geometrical curvature. Due to the short passage before the impeller inlet, only little energy can

be added to the fluid transformed from the blade mechanical energy, which is not enough to compensate the internal energy decline caused by flow acceleration. Or the speed of CO_2 working fluid is very high, the impeller does not have time to work on fluid. The sCO_2 may slip into two-phase region and condensation might take place in those regions. The condensation place is marked out in Fig.9(c), the maximum CO_2 liquid volume fraction is 2.91e-5. As the working fluid continues to flow through the passage, the impeller work on the fluid, which causes a temperature and pressure rise above the critical point, and the condensation disappears.

The aforementioned findings demonstrate that the simulation of a sCO2 compressor can effectively employ the condensation model and two-phase flow simulation method. This method will be applied in the next section to investigate the quantitative impact of phase-change on the compressor's aerodynamic performance at various inlet conditions.

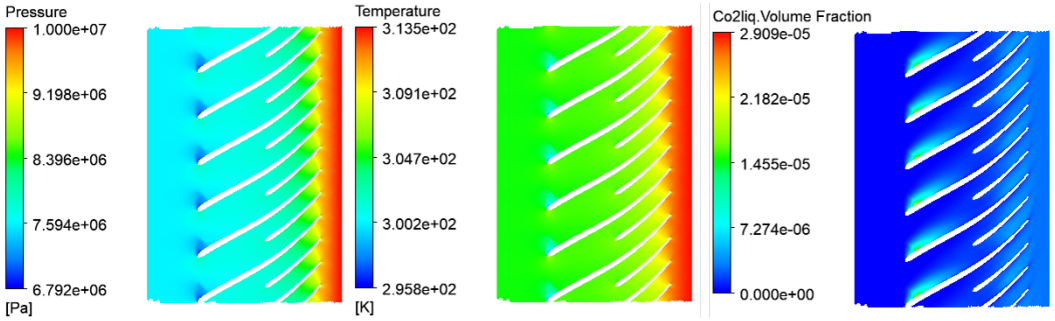

(a) (b) (c)

Fig.9 Contour maps at 50% span(a) pressure;(b) temperature;(c) volume fraction of liquid CO_2

COMPRESSOR OF AN 8MWT SCO2 POWER CYCLE TEST RIG

Simulations about a two-stage centrifugal compressor for an 8MWt sCO_2 power cycle test rig were carried out in this section. The design parameters of main compressor are shown in Table 4. The one-dimensional and three-dimensional diagram of centrifugal impeller are shown in Fig.10. The first stage of the main compressor has 7 main blades and 7 splitters, the return channel has 15 blades and the second stage has 8 main blades and 8 splitters. The splitters can reduce the choke at the impeller. In order to obtain a wide operation range, a vanless diffuser is used.

Table 4

Parameters	Unit	Value
Mass flow rate	Kg/s	26.0
Inlet pressure	MPa	8.0
Inlet temperature	K	306.15
Outlet pressure	MPa	24.0
Rotation speed	Rpm	25000
Pressure ratio	-	3.0
Choke mass flow rate at rated rotation speed	Kg/s	30.5
Surge mass flow rate at rated rotation speed	Kg/s	17.5

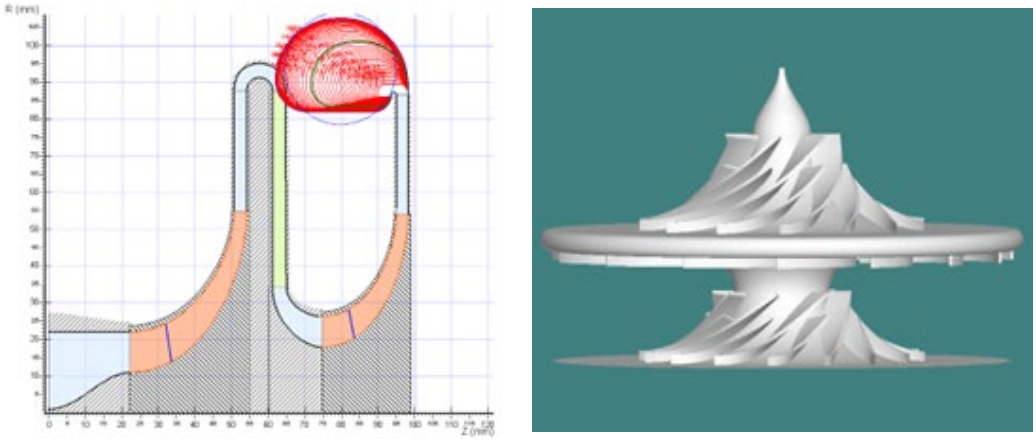

Fig.10 1D(left) and 3D(right) design diagram of centrifugal impeller

The same numerical solver and setting are used in this compressor. The fluid domains of the first and second stage are set as rotating domain with the same rotating speed. The fluid domain of return channel is set as static.

The overall aerodynamic performance of the compressor at design point is assessed in Fig.4 in terms of pressure ratio and efficiency. The rotation speed N is 25krpm and five rotation speeds were chosen. In the simulation, the back pressure was adjusted to alter the compressor mass flow rate. At low rotation speed and mass flow rate, the pressure ratio is relatively small and the stable operation range will be narrower. The pressure ratio from the simulations shows a nearly linear depended on the mass flow rate. With the increase of rotation speed, the pressure ratio increase. However, the simulation stability issues are encountered for the large mass flow rate, leading a rapid decline in efficiency. The main efficiency error of the numerical simulation in this paper results from the fact that the influence of volute on compressor is not considered.

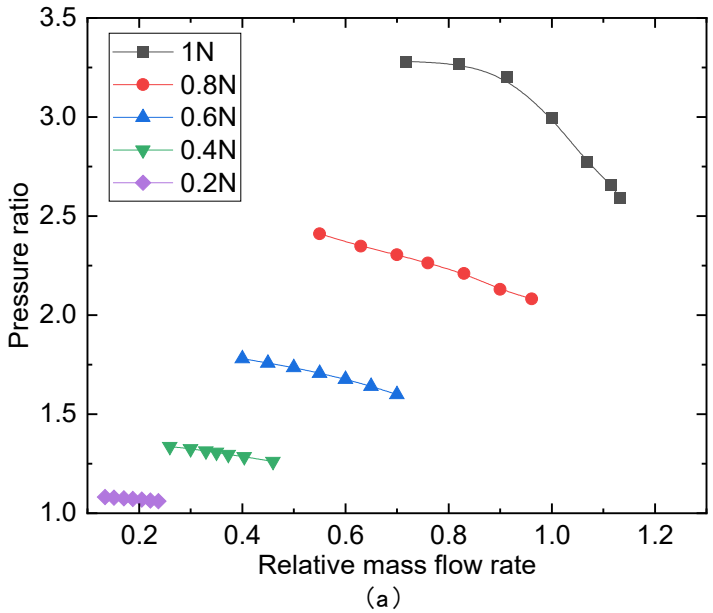

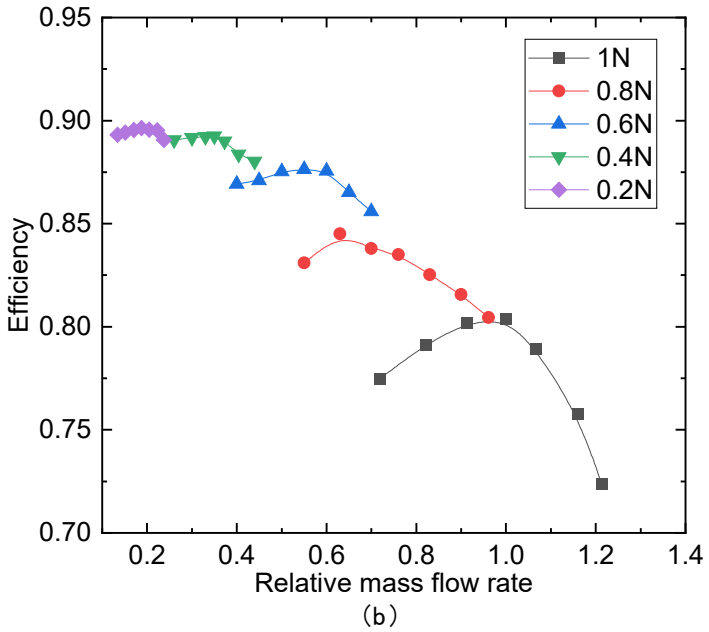

Fig.11 Main compressor performance curve:(a) pressure ration;(b) efficiency

This section concentrates on the specific internal flow field of the compressor at various inlet conditions. Assuming isothermal lines at 306.15K and 313.15K, corresponding to low-temperature and low-temperature, 17 exemplary inlet conditions were taken into consideration, where the relatively entropy varies from 0.829 to 1.575. The detailed information is shown in Table 5 and the inlet points are plotted in T-S diagram in Fig.12. The black solid line is the saturation line.

Table 5 Inlet condition of main compressor

Case	P_t （MPa）	T_t （K）	S （$J/kg \cdot K$）	S_t/S_C
1	15.000	306.15	1.1879	0.829
2	12.000	306.15	1.2216	0.852
3	10.000	306.15	1.2558	0.876
4	12.500	313.15	1.2828	0.895
5	9.003	306.15	1.2828	0.895
6	8.000	306.15	1.3421	0.936
7	10.000	313.5	1.3627	0.951
8	7.786	306.15	1.3906	0.970
9	9.320	313.15	1.4092	0.983
10	9.136	313.5	1.4479	1.010
11	7.700	306.15	1.4756	1.029
12	8.800	313.15	1.5058	1.050
13	7.673	306.15	1.5058	1.050
14	7.600	306.15	1.555	1.085

15	8.500	313.15	1.575	1.099
16	7.600	309.15	1.6490	1.150
17	7.500	313.15	1.7169	1.198

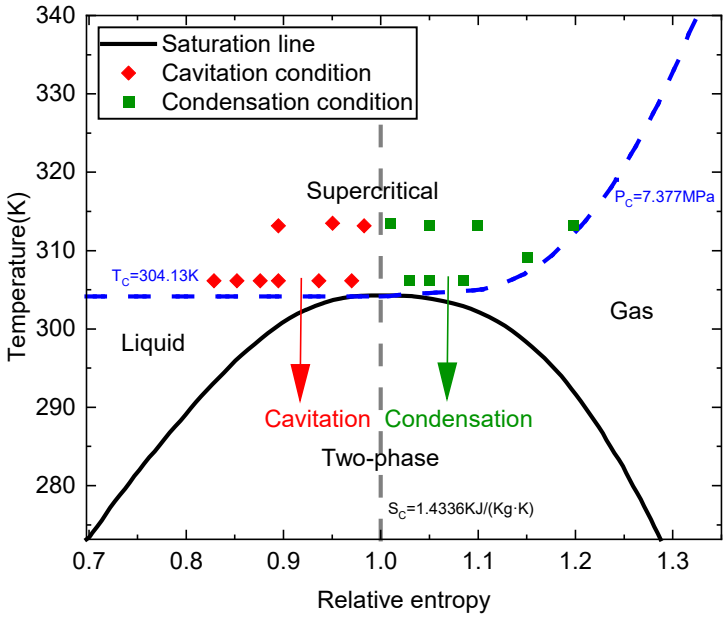

Fig.12 Relative entropy-temperature state diagram of the CO_2

As we all known, the intake of a compressor features nearly isentropic suction phenomena. If the relative entropy is smaller than one, the sCO_2 fluid behaves like liquid. The working fluid will first pass through the liquid region and then penetrate within the two-phase region; moreover, the phase-change occurs as cavitation. The compressor has a large pressure ratio and small temperature rise, reflecting the characteristics of pump. The small temperature rise is consistent with the fact that compressibility in liquid states is low. Performance curves for the inlet relative smaller than one illustrated in Fig. 13, it can be seen that the pressure ratio increase with the increase of relative entropy in general. The surge mass flow rate is nearly the same but the choking-limit mass flow rate decreases with the increase of the relative entropy, since the drop in the speed of sound. The simulation indicates that at high mass flow rate the flow may turn into transonic flow. As the mass flow rate increases, the suction on the pressure side will suddenly increase and the front loading will also increase. What is more, the cavitation become more severe and a wide range of two-phase region come into being at the leading edge of the splitter. As this region grows, the two-phase region is wider enough to cover the channel, resulting in the blockage. The same phenomenon will happen with the increases of the relative entropy of inlet. The simulations indicate that the volume fraction of the vapor CO_2 becomes larger with the increase of the relative entropy. The cavitation does not occur at the inlet relative entropy smaller than 0.876.

If the relative entropy is greater than the critical point, the working fluid will pass through the gas region rather than liquid region and then arrive at the two-phase region. The sCO_2 fluid behaves like gas. In this situation, the phase-change occurs as condensation. The temperature rise is large since the compressibility of the fluid. The low density of the fluid results in a significantly low dimensional pressure rise in the compressor. Performance curves of the various inlet

conditions are illustrated in Fig. 14, it can be seen that the pressure ratio increase with the increase of relative entropy in general but the stable operation mass flow rate becomes smaller since the density decrease with the relative entropy. The condensation disappears at inlet relative entropy of 1.198 and low mass flow rate. When the mass flow rate becomes 10.867 kg/s, the liquid CO_2 volume fraction drops suddenly from 1.03e-5 to 8.97e-10. As the mass flow rate decreases, the liquid CO_2 disappear totally. However, when the condensation disappears, the level of entropy is greater than the cavitation, which means it is easier to condense comparing to the cavitation.

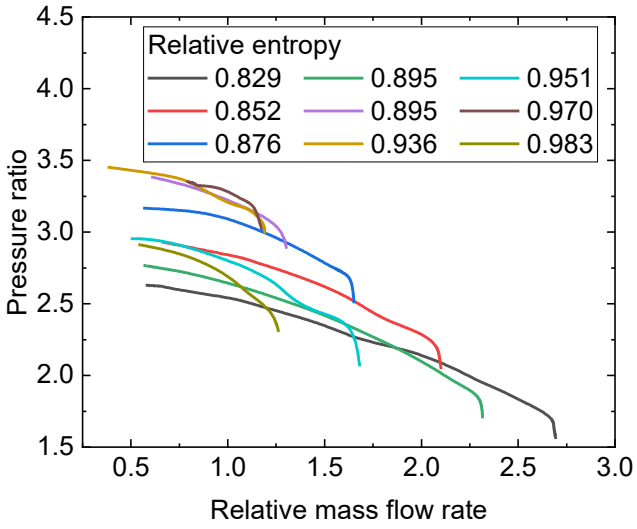

Fig.13 Performance curve at relative entropy smaller than one

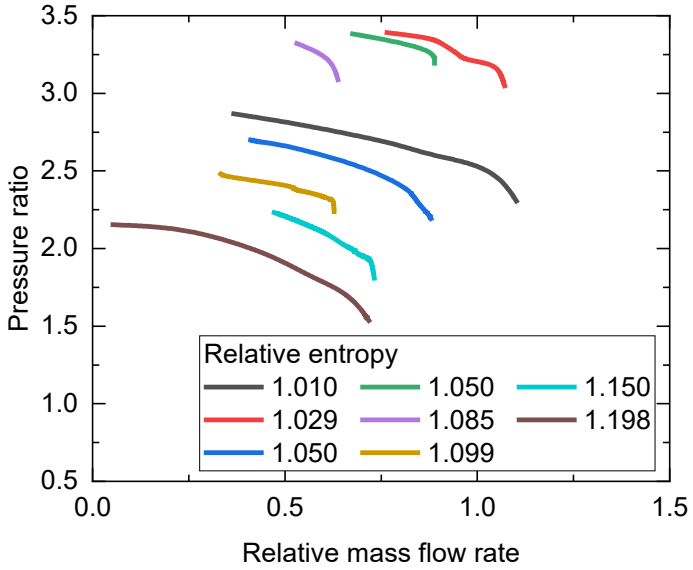

Fig. 14 Performance curve at relative entropy greater than one

Two realistic thermodynamic states are now simulated, with the same relative entropy. These two conditions are representative of respectively high (case 4) and low (case 5) temperature.

Fig. 15 illustrates the contours of the temperature, pressure, vapor volume fraction of CO_2 and density on the blade-to-blade surface at 90% span for case4 and 5. The pressure of the CO_2 working fluid progressively increase along the flow passage throughout the first stage and the total pressure at the exit of the first stage is roughly 1.95 times greater than the inlet pressure. After that the fluid will go through the return channel with a little bit pressure drop and then go through the second stage with a pressure rise. The trend of temperature is similar to the pressure. On the whole, the temperature rise along the flow passage. However, there will be a local low temperature and pressure region in the leading edge of the blade. This phenomenon occurs in both of the first and second stage, since the acceleration in the leading edge of the blade. There are three main reasons causing the acceleration, which are the incidence, loading on the front suction side and choke of the leading edge. After the pressure and temperature rise in the first stage, the inlet temperature and pressure are very high. Therefore, the low temperature and pressure region of the second stage are far away from the critical point, the phase-change will not occur in the second stage. A local low temperature and pressure region also developed at the tail of the blade as a result of the fluid mixing on the pressure side and suction side of the main blade tail. Due to the nonequilibrium phase change effect, cavitation does not occur in the leading edge of the blade, even if the local low temperature and pressure region at case 4 is below the critical point. A well-defined region of low density is observed at the leading edge and the trailing edge of the blade at case 5, which can indicate the occurs of cavitation. The cavitation occurs on the suction side and the suction occurs on the upstream which result from the choke. What is more, the front loading may trigger the cavitation. A sharp decline of pressure takes place which prompts s sudden drop in the speed of sound. And then the relative Mach number is suddenly rising, which turns to cause the blockage, which can be seen in Fig. 16.

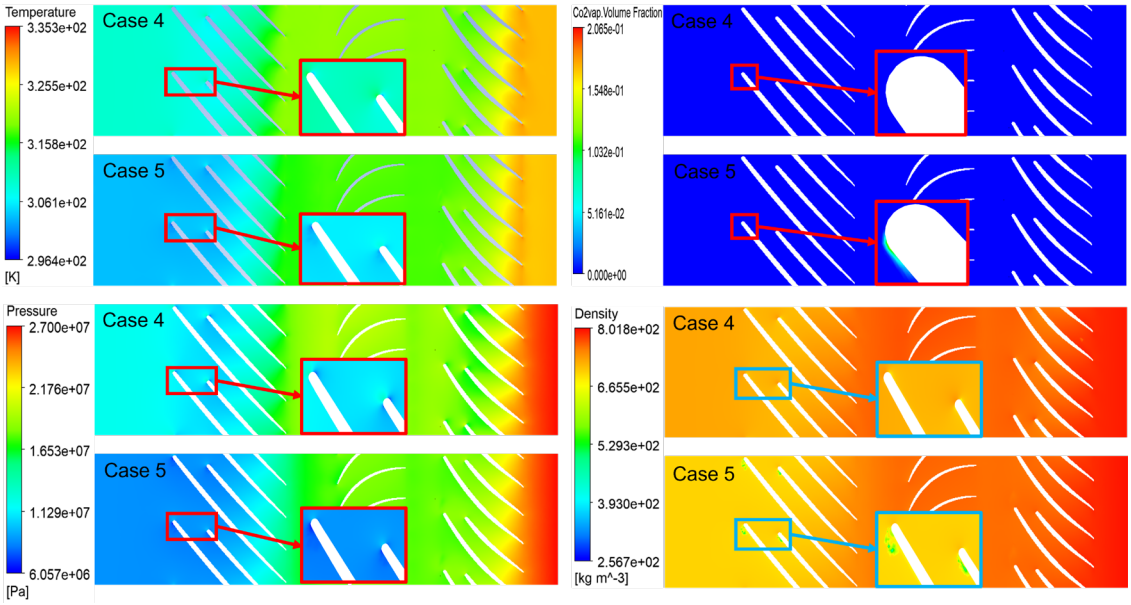

Fig.15 Contours of compressor at 90% span for case 4 and 5

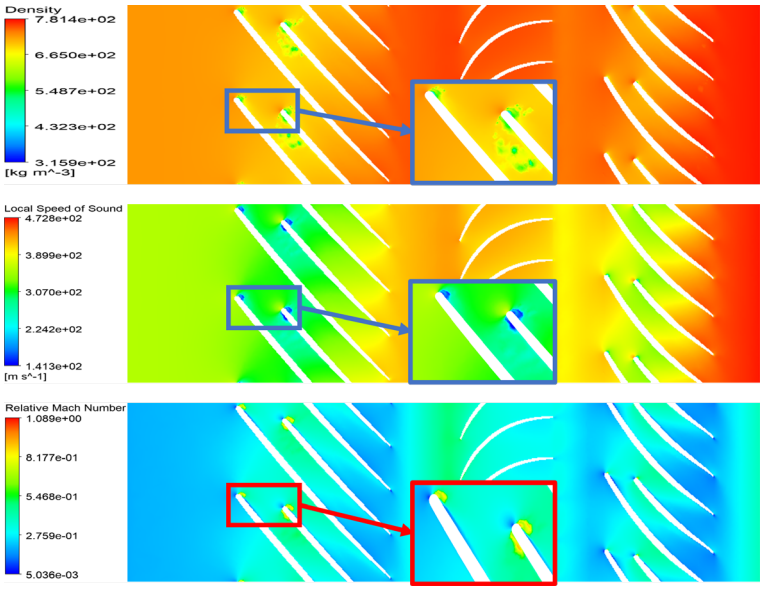

Fig.16 Contours of compressor at 90% span for large mass flow rate

CONCLUSION

In this paper, a series of simulations of a sCO_2 centrifugal compressor operating in various inlet conditions are carried out. The phase-change includes cavitation and condensation, occurring in the leading edge of the blades. The quantitative effect of nonequilibrium phase-change on the performance of sCO_2 centrifugal compressor is investigated. Here comes the conclusions:

1)The supercritical and subcritical thermophysical properties of CO_2 are included in the real gas property table, the properties of the two-phase region are well considered. The metastable properties are calculated by the inverse interpolation. The condensation onset and Wilson line are well predicted, using the nonequilibrium condensation model in conjunction with the RGP table. The performance curve of Sandia is in good agreement with the experiment data.

2)If the inlet relative entropy is smaller than one, the sCO_2 behaves like liquid. The phase-change occurs as cavitation on the leading edge of the blade. Pressure ration increase with the increase of relative entropy. But the choking-limit mass flow rate decrease, since the drop in the speed of sound. As the relative entropy increase, the cavitation becomes severer, which resulting in wide range of two-phase region. When this two-phase region grows wider enough to cover the channel, the choke will soon happen. If the inlet relative entropy is greater than one, the sCO_2 behaves like gas. The phase-change occurs as condensation. The stable operation range will move to the small mass flow as whole, since the small density. It is easier to condense comparing to cavitation for the same entropy level.

REFERENCES

[1] LIU Chenguang; ZHANG Lei. Research Progress of Supercritical Carbon Dioxide Centrifugal Compressor[J]. Thermal Power Generation, 2021, 50(5): 34-42.

[2] BALTADJIEV N D, LETTIERI C, SPAKOVSZKY Z S. An Investigation of Real Gas Effects in Supercritical CO2 Centrifugal Compressors [J]. J Turbomach-Trans ASME, 2015, 137(9): 13.

[3] WRIGHT S, RADEL R, VERNON M, et al. Operation and analysis of a supercritical CO2 Brayton cycle [R]: Office of Scientific and Technical Information (OSTI), 2010.

[4] NOALL J S, NICHOLS B, PASCH J J. Achievable Efficiency and Stability of Supercritical

CO2 Compression Systems, F, 2014 [C].
[5] ALLISON T C, MCCLUNG A, ASME. LIMITING INLET CONDITIONS FOR PHASE CHANGE AVOIDANCE IN SUPERCRITICAL CO2 COMPRESSORS; proceedings of the ASME Turbo Expo: Turbomachinery Technical Conference and Exposition, Phoenix, AZ, F Jun 17-21, 2019 [C]. Amer Soc Mechanical Engineers: NEW YORK, 2019.
[6] LETTIERI C, SPAKOVSZKY Z, PAXSON D, et al. Characterization of non-equilibrium condensation of supercritical carbon dioxide in a de Laval nozzle; proceedings of the ASME Turbo Expo 2017: Turbomachinery Technical Conference and Exposition, GT 2017, F, 2017 [C]. American Society of Mechanical Engineers (ASME).
[7] LETTIERI C, YANG D, SPAKOVSZKY Z. An Investigation of Condensation Effects in Supercritical Carbon Dioxide Compressors [J]. J Eng Gas Turbines Power-Trans ASME, 2015, 137(8): 8.
[8] BRINCKMAN K W, HOSANGADI A, LIU Z S, et al. NUMERICAL SIMULATION OF NON-EQUILIBRIUM CONDENSATION IN SUPERCRITICAL CO2 COMPRESSORS; proceedings of the ASME Turbo Expo: Turbomachinery Technical Conference and Exposition, Phoenix, AZ, F Jun 17-21, 2019 [C]. Amer Soc Mechanical Engineers: NEW YORK, 2019.

ACKNOWLEDGEMENTS

Thanks to National Natural Science Foundation of China (No.52006216) and CAS Project for Young Scientists in Basic Research (No. YSBR-043).